Inorganic Chemistry

Article

pubs.acs.org/IC

Room-Temperature Synthesis of Flower-Like BiOX (X=Cl, Br, I) Hierarchical Structures and Their Visible-Light Photocatalytic Activity

Lang Chen,[†] Rui Huang,[†] Miao Xiong,[†] Qing Yuan,[†] Jie He,[†] Jing Jia,[†] Meng-Yuan Yao,[†] Sheng-Lian Luo,[†] Chak-Tong Au,[†,‡] and Shuang-Feng Yin*[,†]

[†]State Key Laboratory of Chemo/Biosensing and Chemometrics, College of Chemistry and Chemical Engineering, Hunan University, Changsha, Hunan 410082, People's Republic of China

[‡]Department of Chemistry, Hong Kong Baptist University, Room T1214, Cha Chi-ming Science Tower, Kowloon Tong, Hong Kong

Supporting Information

ABSTRACT: A simple method for facile synthesis of three-dimensional (3D) bismuth oxyhalide (BiOX, X=Cl, Br, I) hierarchical structures at room temperature has been developed. Under the influence of L-lysine surfactant, the bismuth and halogen (Cl, Br, I) sources hydrolyze and self-assemble into flower-like hierarchical architectures within 10 min. The resulted materials were characterized by XRD, FESEM, TEM, UV−vis DRS, and N_2 adsorption−desorption techniques. We found that L-lysine is indispensable for their formation and the amount of HX has great effect on the final morphology. The BiOX (X=Cl, Br, I) hierarchical architectures are composed of single-crystalline nanoplates. We propose an amino-and-carboxyl structure-directing mechanism for the formation of the hierarchical structures. To evaluate the photocatalytic activity of the as-prepared materials, rhodamine-B was employed as a probe dye for degradation under visible light. All of the BiOX (X=Cl, Br, I) with 3D architectures show higher photocatalytic activities than their sheet-like counterparts. The superior activity is ascribed to the better light-harvesting capacity of the 3D hierarchical structures. The adopted method can be applied for large-scale generation of novel structures of similar kinds in a facile manner.

INTRODUCTION

The use of photocatalytic techniques to solve energy and pollution problems has attracted much attention. For example, it is considered to be economical as well as beneficial to use photocatalysts to split water and to dematerialise pollutants.[1−3] Nonetheless, the essence of the techniques is the development of effective and environmentally-benign photocatalysts that can absorb visible light (45% of solar energy) for such functionalities. It is hence imperative to search for materials (mostly semiconductors) that are ecologically safe and can act as high-efficacy photocatalysts.

Bismuth is a kind of p-block metal with a d^{10} configuration. For Bi^{3+}-based oxides, there is the hybridization of Bi6s and O2p levels and the formation of a hybridized valence band (VB) that favors the mobility of photogenerated holes.[4,5] Bismuth oxyhalides are ternary compounds widely used as photocatalysts.[6−9] It was Zhang and coauthors who first reported that BiOCl exhibits better performance than TiO_2 in the photocatalytic degradation of methylene orange.[6] Most of the photocatalysts are in the form of nanomaterials. It is known that the unique properties of nanomaterials are dependent on the shape, structure, phase, size, size distribution, and crystal facets as well as the ways they are prepared, such as the primary building blocks and how the building blocks are assembled or integrated.[9−18] In view of that, efforts were paid for the controllable formation of nanomaterials, and BiOX of different morphologies were synthesized by numerous methods. Although well-defined BiOX nanostructures, such as hierarchical nanoplates, nanoparticles, and nanobelts have been fabricated,[6−9,19−23] the adopted methods have shortcomings. For example, long synthesis time, high reaction temperature, and/or use of toxic organic solvents are common in hydro- and/or solvo-thermal approaches; and complicate equipments are required in sonochemical, electrospinning, and low-temperature chemical vapor transport methods. It is hence of great importance to develop synthesis methods that are simple and facile. In other words, the methods have to be conducted under mild conditions without the need of organic precursors or solvents. For industrial applications, it is good to have the BiOX structures broadened and the related synthesis controllable for a specific morphology. Furthermore, the process has to be environmentally-benign. Very recently, Gnayem and Sasson reported a simple method for the preparation of 3D flower-like $BiOCl_xBr_{1-x}$.[24] Nonetheless, there is still no report on a facile

Received: May 29, 2013
Published: September 19, 2013

   dx.doi.org/10.1021/ic401349j | Inorg. Chem. 2013, 52, 11118−11125

method that can be used for the preparation of 3D flower-like hierarchical BiOCl, BiOBr, and BiOI.

It is known that facets of a crystal are different in geometric as well as electronic structures. Depending on crystallographic orientation, a facet exhibits intrinsic reactivity as well as unique surface physical and chemical properties.[25] However, the preparation of crystals specific in crystal facets is always a challenge, especially the synthesis process has to be conducted at room temperature and be completed in a short period of time.[17,26−29] Recently, we reported a facile synthetic pathway for the preparation of single-crystalline BiOCl nanoflowers.[30] Lately, we employed environment-benign L-lysine, a nontoxic biomolecular surfactant, as structure-directing agent. Using $Bi(NO_3)_3{\cdot}5H_2O$ and HX as Bi and X sources and under the influence of L-lysine, hierarchical BiOX can be easily synthesized in an aqueous medium at room temperature within 10 min. The as-prepared BiOX materials are composed of single-crystalline nanoplates with oriented growth along the (110) face. In this work, we report the controllable growth of BiOX and propose a mechanism appropriate for the formation of this family of hierarchical materials.

EXPERIMENTAL SECTION

Synthesis. All of the reagents were analytical grade and commercially available. They were used without further purification. Typically, 10 mmol of $Bi(NO_3)_3{\cdot}5H_2O$ (4.85g) and 0.4 g of L-lysine were dissolved in concentrated HX solution (X=Cl, Br, I; HCl: 36.5 wt.%, HBr: 40 wt. % and HI: 57 wt. %; keeping a Bi/X molar ratio of 1, 1/2, or 1/3). Then the mixture was quickly diluted to 100 mL by water for the immediate formation of precipitates. After the solution was adjusted to pH = 9 by adding 5 wt. % ammonia solution, the BiOX products were collected and washed with water and alcohol, and dried at 80 °C for 4 h.

Characterization. The BiOX materials in the form of crystals were collected and characterized by powder X-ray diffraction (XRD) on a Bruker Automatic Diffractometer (Bruker D8 Advance) with monochromatized CuKα radiation (λ = 0.154 06 nm) at a setting of 40 kV and 80 mA. The scanning rate was 0.02° (2θ)/s and the scanning range was 5−75°. X-ray photoelectron spectroscopy (XPS) was employed for the measurement of surface composition and chemical states of BiOX. The micro- and nanostructure as well as the morphology of as-prepared samples was examined using a field emission scanning electron microscope (FE-SEM) (Hitachi S-4800). Transmission electron microscopy (TEM) and high-resolution transmission electron microscopy (HRTEM) as well as selected area electron diffraction (SAED) images were taken over a JEM-3010F transmission electron microscope at an accelerating voltage of 200 kV. The BET surface area was measured using a Quantachrome NovaWin instrument. UV−vis diffuse reflectance spectra (UV−vis DRS) of samples were obtained over a UV−vis spectrophotometer (Cary 300) using $BaSO_4$ as reference.

Catalyst Evaluation. Degradation of Rhodamine-B (Rh−B) was used as probe reaction to evaluate the photocatalytic activity of the as-synthesized BiOX samples. Photodegradation processes were conducted using a homemade Pyrex glass vessel with temperature being maintained at room temperature by means of an external water flow as described elsewhere.[30]

RESULTS AND DISCUSSION

Phase Structure. Figure 1 shows the XRD patterns of the BiOX (X=Cl, Br, I) samples. The patterns for BiOCl, BiOBr, and BiOI can be indexed to tetragonal phases (BiOCl JCPDS Card No. 06-0249; BiOBr: 09-0393 and BiOI: 73-2062). No signals other than those of the BiOX phases can be detected, indicating that the samples are phase-pure. Despite the phase purity of the bismuth oxyhalides, the peak intensities disagree

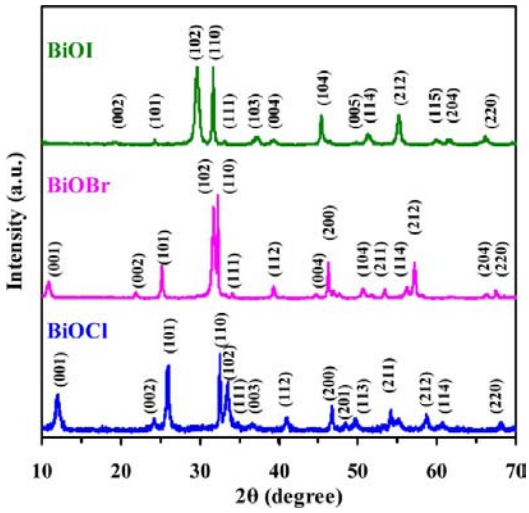

Figure 1. XRD patterns of BiOX (X=Cl, Br, I) samples.

with those of the JCPDS cards. The intensity of the (110) peaks of the as-prepared BiOX samples are as high as or even higher than those of the (102) peaks. The (110)/(102) intensity ratios of the as-prepared BiOCl, BiOBr, and BiOI are 1.54, 0.99, and 0.99, whereas those based on JCPDS data for polycrystalline samples are 0.79, 0.65, and 0.55 (Table 1). It is known that a rise in intensity of a particular diffraction peak implies a better exposure of planes that cause the reflection. In other words, there is anisotropic growth along the (110) faces during the synthesis of the as-prepared samples.[32]

Table 1. (110)/(102) Intensity Ratios of Samples

	(110)/(102)	JCPDS data
BiOCl	1.54	0.79
BiOBr	0.99	0.65
BiOI	0.99	0.55

Surface Composition. Herein, BiOBr is taken as an example to illustrate the results of XPS analysis. The relevant XPS peak position is calibrated against the C1s signal of contaminant carbon at a binding energy of 284.6 eV. Figure 2(a) is a typical survey spectrum, and only Bi, O, Br and trace amount of C are detected, indicating that the high purity of BiOBr. Figure 2, parts (b)−(e) show the Bi4f, Br3d, O1s, and N1s spectra, respectively. The $Bi4f_{7/2}$ and $Bi4f_{5/2}$ peaks at 159.0 and 164.2 eV, respectively, are characteristic of Bi^{3+} (Figure 2(b)). The peak located at 68.5 eV can be ascribed to Br3d signal (Figure 2(c)). There are two kinds of oxygen species with O1s signals at 530.1 and 532.5 eV; the former is ascribed to layer-structured BiO and the latter to surface hydroxyl (or crystal water) (Figure 2(d)). There is no detection of N1s signal (Figure 2(e)), indicating the complete removal of L-lysine and NO_3^-. On the basis of the XRD and XPS results, it is reasonable to state that BiOX (X=Cl, Br, I) can be prepared by the adopted method.

Morphological Structure. The SEM images of BiOX (X=Cl, Br, I) are presented in Figure 3. As can be seen from the low- and high-magnification pictures, the fabricated BiOX samples are of flower-like 3D hierarchical structures, having radially grown nanoplates about 30 nm in thickness. The nanoplates stacked and intercrossed with one another, forming a lot of nano- and macro-pores on the surface. It is known that

dx.doi.org/10.1021/ic401349j | Inorg. Chem. 2013, 52, 11118−11125

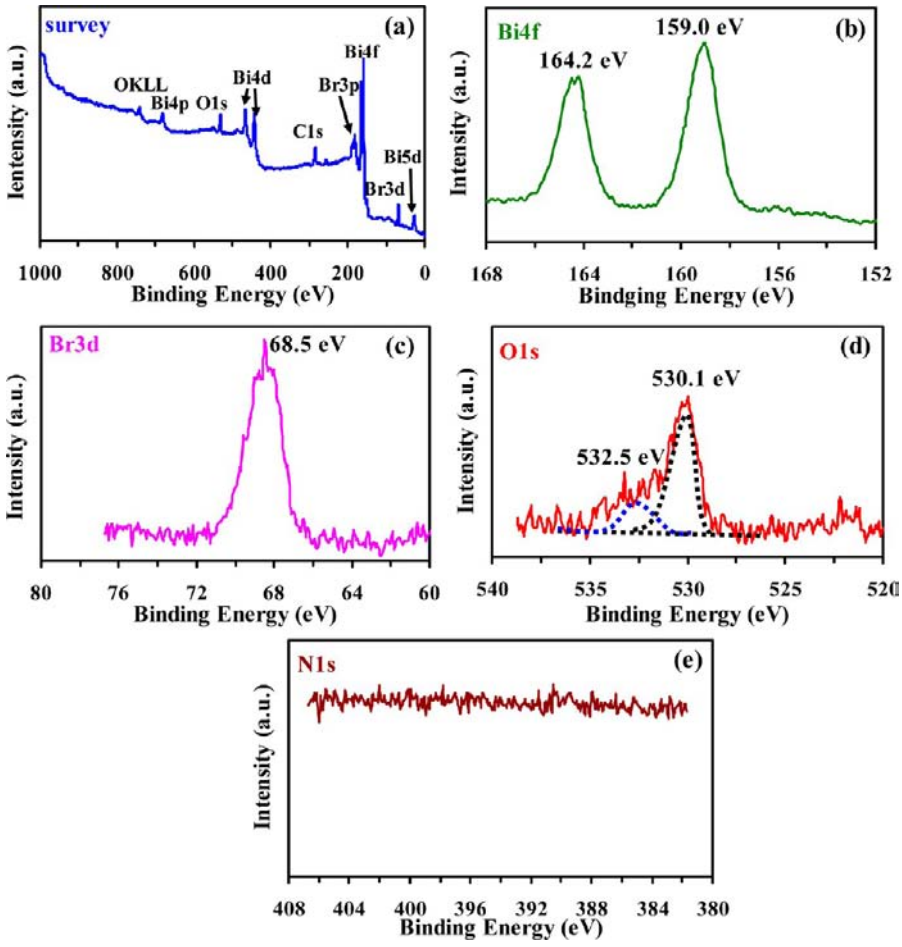

Figure 2. XPS spectra of BiOBr prepared using L-lysine as surfactant, (a) survey scan, (b) Bi4f, (c) Br3d, (d) O1s, and (e) N1s spectra.

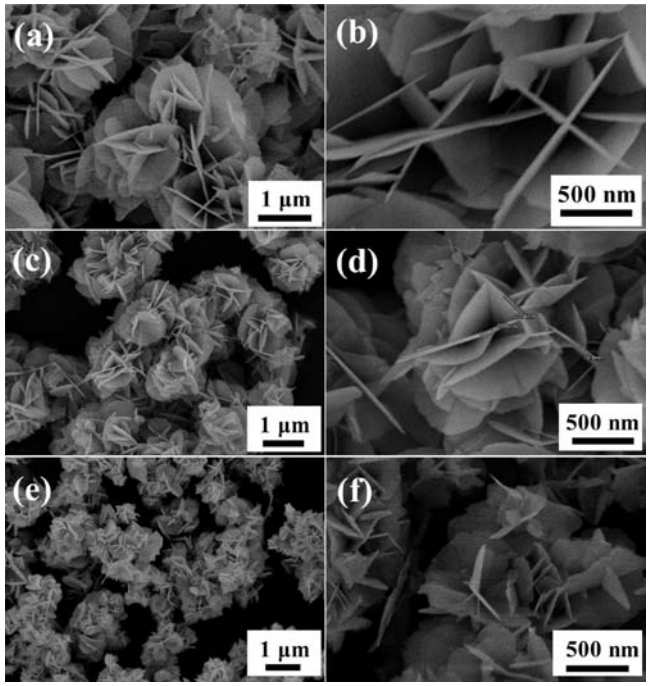

Figure 3. SEM images of (a)(b) BiOCl, (c)(d) BiOBr, and (e)(f) BiOI.

the presence of pores and thin nanoplates are beneficial for light harvesting and separation of photogenerated electron–hole pairs; both are factors for the promotion of photocatalytic activity.

As shown in Figure 4, the TEM pictures also reveal that the flower-like 3D hierarchical structures are composed of thin nanosheets. The HRTEM image (Figure 4(d)) confirms the high crystallinity of BiOBr, showing ordered lattice fringes with interplanar spacing of 0.278 nm corresponding to (110) planes (JCPDS card No. 09–0393). The observation is in good

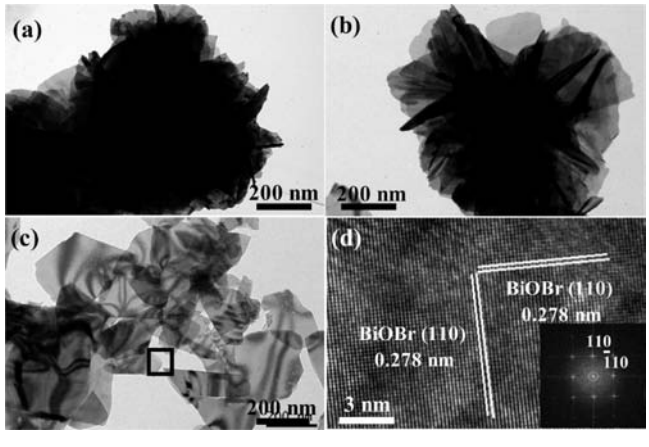

Figure 4. (a)–(c) TEM and (d) HRTEM images of BiOBr sample.

dx.doi.org/10.1021/ic401349j | Inorg. Chem. 2013, 52, 11118–11125

agreement with the XRD result that the nanoplates grow along the (110) planes. The SAED pattern (inset of Figure 4(d)) of an individual nanosheet shows well-defined diffraction spots, indicating single crystallinity. The bright spots can be indexed to the (110) planes of tetragonal BiOBr crystal, in agreement with the XRD results that the nanosheets grow along the (110) planes. The observations are similar to those of BiOCl reported in our previous work.[30]

Effect of Reaction Conditions and Plausible Growth Mechanism. With the assistance of L-lysine, BiOX samples of flower-like 3D hierarchical structures can be synthesized facilely at room temperature in water within several minutes. We found that despite synthesis time has little effect on product microstructure, factors such as the amount of precursors and kind of surfactants pose an influence on the final morphology.

Amount of HBr. The influence of varying the amount of HBr was studied, and the SEM images of the resulted samples are displayed in Figure 5. It is clear that even with L-lysine being the

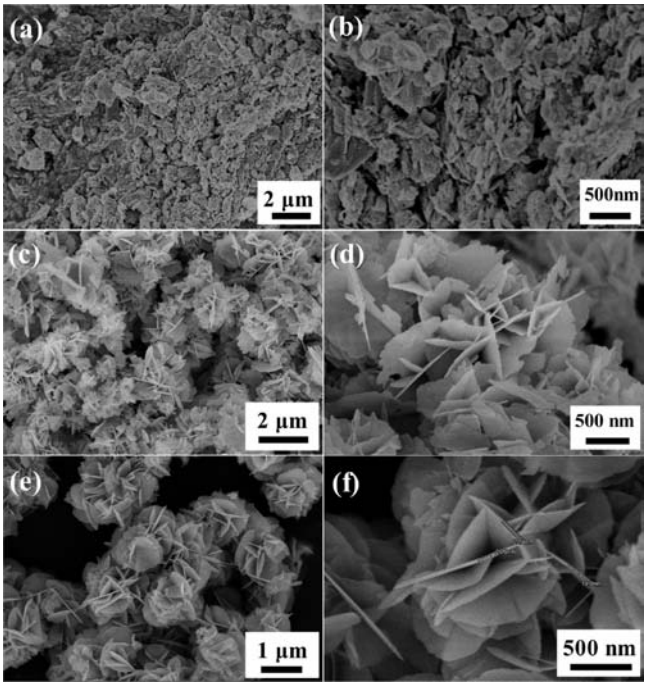

Figure 5. SEM images of BiOBr samples prepared (L-lysine as surfactant) at Bi/Br mole ratio of (a),(b) 1/1, (c),(d) 1/2, and (e),(f) 1/3.

surfactant, only nanosheets are formed at a Bi/Br ratio of 1, and there is no trace of hierarchical structure. At a Bi/Br ratio of 1/2, there is cross as well as assembly of nanosheets and the detection of flower-like structures. At a Bi/Br ratio of 1/3, there is the detection of assembled BiOBr with 3D flower-like hierarchical structures.

Surfactants. Figure 6 shows the SEM images of BiOBr samples prepared using different kinds of surfactants, viz. triblock copolymer Pluronic (F127, 1.0 g), polyvinylpyrrolidone (PVP, 1.0 g), and cetyltrimethyl-ammonium bromide (CTAB, 1.0 g). It is clear that without the assistance of surfactant (Figure 6(a),(b)), there is fast hydrolysis of Bi^{3+} and X^-, and the as-prepared BiOBr is composed of particles of irregular size. When F127 (Figure 6(c),(d)), CTAB (Figure 6(e),(f)) and PVP (Figure 6(g),(h)) are used, the products are composed of nanosheets, and the sheets pile up to give a fish-scale-like morphology. As demonstrated before, when L-lysine is used as surfactant, there is the formation of 3D flower-like hierarchical structures. Compared to F127, CTAB, and PVP, L-lysine is unique because it possesses both carboxyl and amino groups that reacts simultaneously with Bi^{3+} and halide ions, respectively. We used glutamic acid (Gly, 0.4 g) that also possesses both carboxyl and amino as surfactant and obtained 3D hierarchical structures (Figure 6(i),(j)) similar to those formed when L-lysine is used. Interestingly, if a mixture of 1,2-ethanediamine and acetic acid (EA, 0.16 g + HAc, 0.46 g 36 wt. %) is employed as surfactant, then the product (Figure 6(k),(l)) shows unique 3D hierarchical structures composed with dozens of intercrossed nanosheets but there is no sight of flower-like morphology. It is believed that despite EA and HAc provide carboxyl and amino groups they are too far apart and fail to become a growth center for the assembling of 3D flower-like structure. In other words, EA and HAc can act like L-lysine to induce the formation of crossed nanoplates but they cannot assemble nanoplates into flower-like structures. It is apparent that the morphologies of BiOX nanomaterials are surfactant dependent.

Possible Formation Mechanism. To be able to control the morphology of BiOX products, it is important to figure out how a surfactant functions as a structure-directing agent.[32,33] On the basis of the experimental results and observations, a possible mechanism for the formation of 3D flower-like BiOX hierarchical structures is proposed (Scheme 1). When $Bi(NO_3)_3{\cdot}5H_2O$ is dissolved in concentrated HX solution, there is no precipitate (eq 1). At Bi:HX molar ratio of 1:3 or 1:2, Bi^{3+} and HX react with L-lysine (eq 2). Upon dilution of the solution with water, there is the hydrolysis of Bi^{3+} as well as the germination of $BiONO_3$ and BiOX crystal nuclei (eqs 3−5) beside the L-lysine molecules. With the adjustment of pH to 9 (by adding ammonia solution), there is promoted formation of $BiONO_3$ and BiOX. Together with the anisotropic growth of BiOX crystals along the (110) planes, there is gradual conversion of $BiONO_3$ to BiOX (eq 6) and accumulation of BiOX nanosheets around L-lysine, forming the 3D flower-like BiOX microstructures through self-assembly. At a Bi:HX molar ratio of 1:1, there is no reaction between L-lysine and X^-. With the addition of water and change of solution pH value, there is fast hydrolysis of Bi^{3+} and X^-. However, unlike the case of Bi:HX = 1:3, the growth of BiOX crystal nuclei occurs only around the carboxyl of L-lysine and there is no formation of intercrossed nanoplates.

$$Bi(NO_3)_3{\cdot}5H_2O + HX \rightarrow Bi^{3+} + X^- + NO_3^- + H^+ \quad (1)$$

$$Bi^{3+} + X^- + \text{L-lysine} \rightarrow Bi^{3+}[\text{L-lysine}^-][X^-]_2 \quad (2)$$

$$Bi^{3+} + NO_3^- + H_2O \rightarrow BiONO_3 + HNO_3 \quad (3)$$

$$Bi^{3+} + X^- + H_2O \rightarrow BiOX + HX \quad (4)$$

$$Bi^{3+}[\text{L-lysine}^-][X^-]_2 + NH_3{\cdot}H_2O \rightarrow BiOX + [\text{L-lysine}^-]NH_4^+ + H_2O \quad (5)$$

$$BiONO_3 + X^- \rightarrow BiOX + NO_3^- \quad (6)$$

Optical Properties. UV−visible diffuse reflectance spectra (UV−vis DRS) was used to study the light absorption properties of BiOX (X═Cl, Br, I). Figure 7(a) shows that the absorption edges of BiOCl, BiOBr, and BiOI are 410, 450,

dx.doi.org/10.1021/ic401349j | Inorg. Chem. 2013, 52, 11118−11125

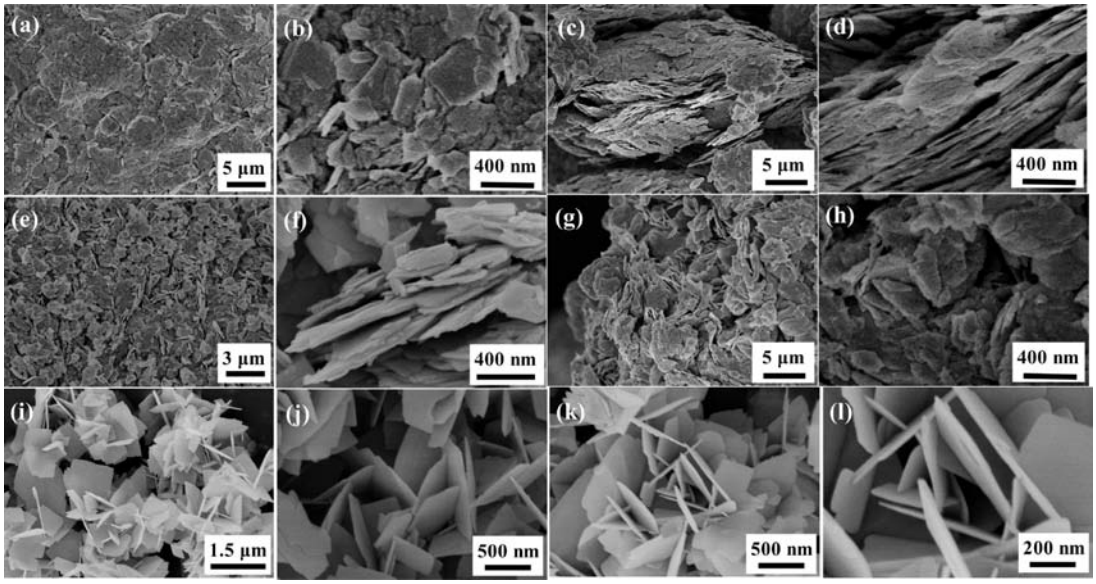

Figure 6. SEM images of BiOBr samples prepared with the assistance of surfactants: (a),(b) none; (c),(d) F127 (1.0 g); (e),(f) CTAB (1.0 g); (g), (h) PVP (1.0 g); (i),(j) Gly (0.4 g); (k),(l) EA (0.16 g) +HAc (0.46 g 36 wt % HAc).

Scheme 1. Possible Formation Mechanism of 3D Flower-Like BiOBr Hierarchical Structures

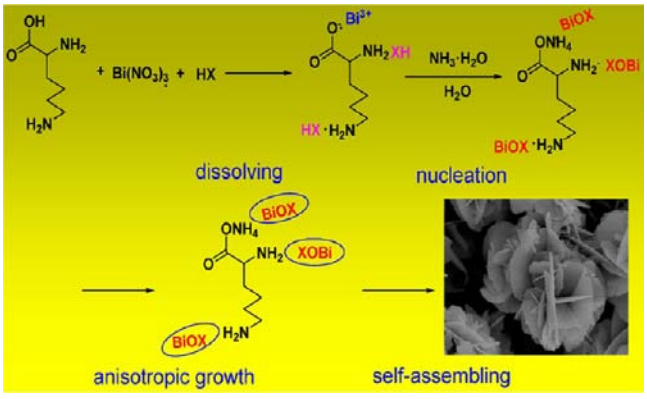

and 690 nm, respectively, indicating that the samples are able to absorb visible light. As BiOX (X=Cl, Br, I) are indirect transition semiconductors, we follow the classical Tauc approach to evaluate their band gaps (Figure 7(b)).[30] For the as-prepared BiOCl, BiOBr, BiOI, they are 2.84, 2.60, 1.69 eV, respectively. The results further confirm that the samples can be excited by visible light.

Nitrogen Adsorption−Desorption. Presented in Figure 8 are the N_2 adsorption−desorption isotherms of the BiOX (X=

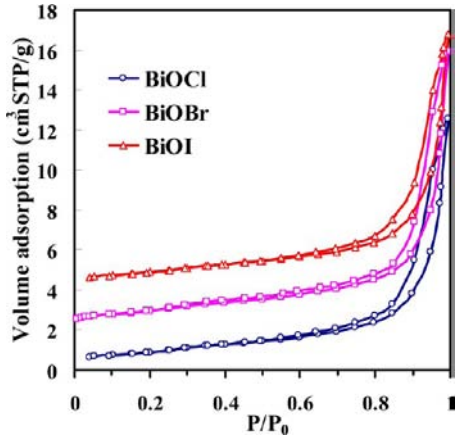

Figure 8. Nitrogen adsorption−desorption isotherms of BiOX (X=Cl, Br, I) samples.

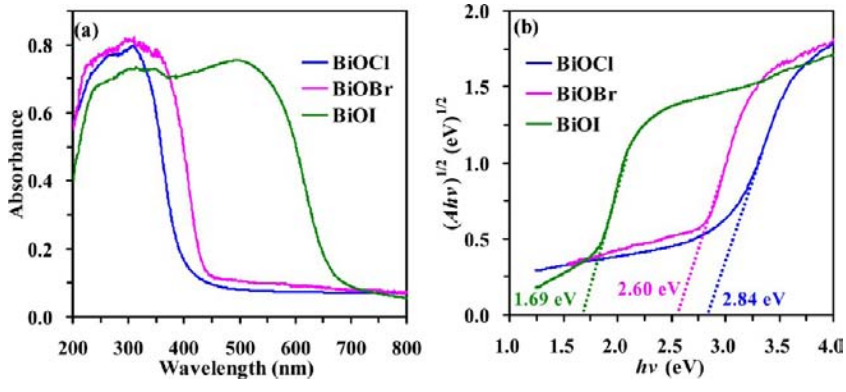

Figure 7. (a) UV−vis absorption spectra and (b) corresponding $(Ahv)^{1/2}$-hv plots of BiOX (X=Cl, Br, I).

dx.doi.org/10.1021/ic401349j | Inorg. Chem. 2013, 52, 11118−11125

Cl, Br, I) samples. One can see type-IV isotherms with hysteresis loops starting at P/P_0 = 0.5 that show high adsorption at high relative pressure (P/P_0 = 1.0), indicating the existence of micropores, mesopores, and macropores. The pore size distributions of the composites were estimated based on the BJH method. The results show that the samples possess pores in the range of 1.5 to 200 nm, and the average pore diameters of BiOCl, BiOBr and BiOI are 2.2, 2.4, and 2.2 nm, respectively. The larger pores that range up to 200 nm are the pores between nanoplates, and their existence can be observed in the SEM images. The specific surface areas of the as-synthesized BiOCl, BiOBr, and BiOI are 12.1, 14.3, and 13.4 m^2/g, respectively. The BET results are in agreement with the SEM results that the samples are similar both in dimension and structure.

Photocatalytic Performance. Photocatalytic degradation of Rhodamine-B (Rh−B) was employed as a probe reaction to investigate the activities of as-synthesized BiOX (X═Cl, Br, I) under the irradiation of visible light ($\lambda \geq 400$ nm). Figure S1 (Supporting Information, SI) depicts the adsorption properties of Rh−B on the BiOX (X═Cl, Br, I) samples without light irradiation. The adsorption−desorption equilibrium between Rh−B and catalysts can be quickly established within 30 min, and 31%, 34%, and 35% of the initial Rh−B was adsorbed on BiOI, BiOBr, and BiOCl, respectively. Figure 9 shows the

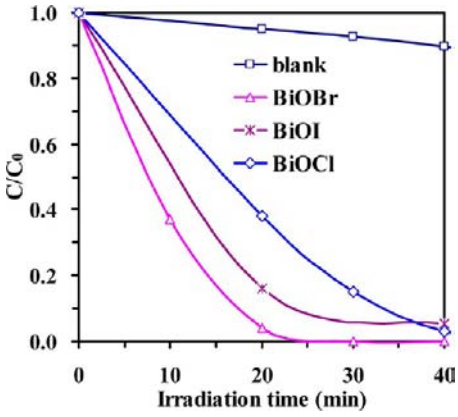

Figure 9. Photocatalytic degradation of Rh−B over the as-prepared BiOX samples under irradiation of visible light ($\lambda \geq 400$ nm).

variation of Rh−B concentration (C/C_0) with irradiation time. The result of Rh−B photolysis (no catalyst) is also shown for comparison, and only 9% of the original Rh−B is removed in 40 min. The photodegradation of Rh−B over BiOCl, BiOBr, and BiOI is 97%, 100%, and 97% within 40 min, respectively, far more significant than that of photolysis. Complete dematerialization of Rh−B is observed after 40 and 60 min over BiOBr and BiOCl, respectively, but dematerialization of Rh−B over BiOI is still not complete (about 97%) after 60 min. The UV−vis absorption of Rh−B vs irradiation time is shown in Figure S2 (SI), and it was observed that the diminution of absorption peaks is gradual. In fact, the diminishing of absorption peaks is accompanied by a shift of peak position to lower wavelength. The results indicate a step-by-step degradation of Rh−B. The degradation of Rh−B over BiOBr is faster than that over BiOCl, which can be ascribed to the narrower band gap of BiOBr in comparison to that of BiOCl. In the case of BiOI, despite there being a shift of absorption peak toward lower wavelengths, the absorption peaks cannot be completely removed even with prolonged irradiation, suggesting that it is not possible to remove Rh−B completely when BiOI is used as a photocatalyst. The result is in agreement with our previous report[34] and that reported by Li et al.,[35] that BiOI shows much lower photocatalytic activity than BiOCl and BiOBr in Rh−B decomposition.

It has been reported that the active species in the photocatalytic degradation process are different across various catalysts, and that ·OH radicals and photogenerated holes are the main active species in oxidation of organic dyes.[36,37] It is reckoned that ·OH is generated from O_2 and electrons or holes according to the following steps:

$$O_2 + e = \cdot O_2^- \quad (7)$$

$$\cdot O_2^- + e + 2H^+ = H_2O_2 \quad (8)$$

$$H_2O_2 + e = \cdot OH + OH^- \quad (9)$$

$$h^+ + OH^- = \cdot OH \quad (10)$$

We employed hole (trietholamine, TEOA) and ·OH (*tert*-butyl alcohol, TBA) scavengers[36,37] to study the active species in the BiOBr and BiOI catalytic systems. The scavengers (kept at 10 mmol/L) were added to the Rh−B solutions together with the catalysts before irradiation. As shown in Figure 10, the

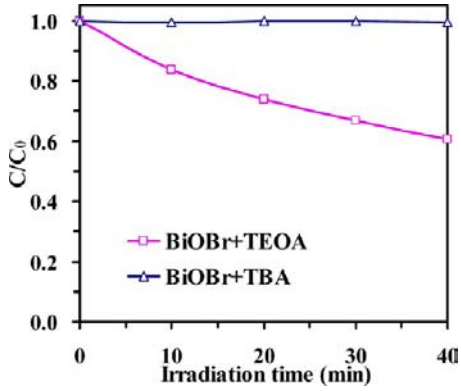

Figure 10. Photocatalytic degradation of Rh−B over the as-prepared BiOBr samples in the presence of scavengers.

degradation of Rh−B decreases from 100% to 40% and from 100% to 4% on BiOBr with the addition of TEOA and TBA, respectively, indicating that the decomposition of Rh−B is mainly due to ·OH, and that both ·OH generated from electrons (eqs 7−9) and holes (eq 10) take part in the Rh−B oxidation process. It is so much different when BiOI is used as catalyst. When the hole scavenger is added to the BiOI system, there is no apparent effect on the degradation process (Figure S3(a), SI), and with the addition of ·OH scavenger, there is hardly any Rh−B degradation within 60 min irradiation (Figure S3(b), SI). The results suggest that the degradation of Rh−B is mainly due to ·OH generated from electrons. It is plausible that the valence band of BiOI is not positive enough for oxidation of H_2O to ·OH as reported in the literature.[31,38,39]

The photocatalytic degradation of Rh−B over BiOBr samples of different morphologies was evaluated, and the results are shown in Figure 11. Over the BiOBr samples prepared using PVP, F127, and CTAB as surfactant, Rh−B removal in 40 min is 73%, 73%, and 71%, respectively. Over the BiOBr sample prepared without the use of any surfactant, Rh−B removal is 69% in 40 min. However, there is complete removal of Rh−B

dx.doi.org/10.1021/ic401349j | Inorg. Chem. 2013, 52, 11118−11125

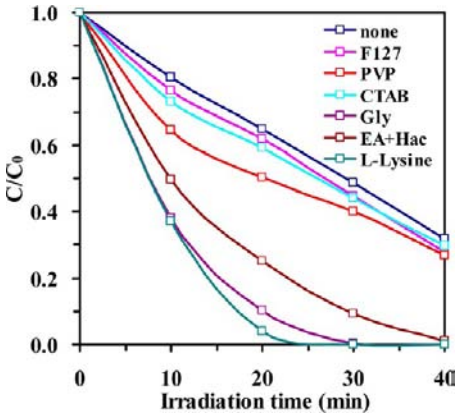

Figure 11. Photocatalytic degradation of Rh−B over the as-prepared BiOBr samples prepared with different surfactants under irradiation of visible light ($\lambda \geq 400$ nm).

in 40 min over the BiOBr samples synthesized employing Gly, EA+Hac, and L-lysine as structure-directing agents. It is reasonable to ascribe the higher photocatalytic activities of the latter samples to their 3D hierarchical structures. To eliminate the adsorption effect of 3D flower-like structure, the degradation rate was evaluated based on the reaction constant (k) determined by plotting $\ln(C/C_e)$ (C_e is the concentration of Rh−B after adsorption−desorption equilibrium) against irradiation time (t). The k values of BiOBr samples prepared with the assistance of Gly, EA+HAc, and L-lysine are 0.100, 0.176, and 0.217 min^{-1}, respectively. The values are much larger than that of the BiOBr sample prepared using PVP (0.027 min^{-1}), F127 (0.027 min^{-1}), and CTAB (0.027 min^{-1}) as surfactants or than that of the BiOBr sample prepared without using any surfactant (0.025 min^{-1}). The results further confirm that the 3D flower-like BiOBr samples are superior to the sheet-like counterparts in terms of photocatalytic activity under visible light irradiation.

CONCLUSIONS

A simple, facile, and environmentally-benign method is introduced for the preparation of 3D flower-like hierarchical BiOX (X=Cl, Br, I). In this method, water is used as solvent and L-lysine as structure-directing agent. We observe anisotropic growth of BiOX single crystals along the (110) planes around L-lysine and the final formation of 3D flower-like structures. It is found that the optimal Bi:X molar ratio is 1:3, and the copresence of carboxyl and amino groups in surfactant is indispensable for the synthesis of 3D flower-like BiOX. On the basis of the experimental results, a possible formation mechanism is proposed for the flower-like hierarchical structures. It was found that the 3D flower-like samples show higher photocatalytic activities than the sheet-like or fish-scale-like counterparts under visible light irradiation.

ASSOCIATED CONTENT

Supporting Information

Adsorption properties of the as-prepared BiOX samples in Rh-B solution without light irradiation (Figure S1); UV-vis absorption of Rh-B vs irradiation time over the as-prepared catalysts (Figure S2); and UV-vis absorption spectra of Rh-B vs irradiation time using BiOI as catalyst upon the use of TEOA and TBA scavengers (Figure S3). This material is available free of charge via the Internet at http://pubs.acs.org.

AUTHOR INFORMATION

Corresponding Author

*Phone: 86-731-88821711. Fax: 86-731-88821171. E-mail: sf_yin@hnu.edu.cn.

Notes

The authors declare no competing financial interest.

ACKNOWLEDGMENTS

This project was financially supported by NSFC (Grant Nos. U1162109, 21273067, and J1210040), the Program for New Century Excellent Talents in Universities (NCET-10-0371), Program for Changjiang Scholars and Innovative Research Team in University (IRT1238), and the Fundamental Research Funds for the Central Universities. C.T.A. thanks the HNU for an adjunct professorship.

REFERENCES

(1) Osterloh, F. E. *Chem. Soc. Rev.* **2013**, *42*, 2294−2320.
(2) Chen, C. C.; Ma, W. H.; Zhao, J. C. *Chem. Soc. Rev.* **2010**, *39*, 4206−4219.
(3) Chen, X. B.; Shen, S. H.; Guo, L. J.; Mao, S. S. *Chem. Rev.* **2010**, *110*, 6503−6570.
(4) Zhang, L. S.; Wang, H. L.; Chen, Z. G.; Wong, P. K.; Liu, J. S. *Appl. Catal., B* **2011**, *106*, 1−13.
(5) Roderick, M. *Angew. Chem., Int. Ed.* **2004**, *43*, 4265−4277.
(6) Ai, Z. H.; Ho, W. K.; Lee, S. C.; Zhang, L. Z. *Environ. Sci. Technol.* **2009**, *43*, 4143−4150.
(7) Zhang, K. L.; Liu, C. M.; Huang, F. Q.; Zheng, C.; Wang, W. D. *Appl. Catal., B* **2006**, *68*, 125−129.
(8) Xia, J. X.; Yin, S.; Li, H. M.; Xu, H.; Yan, Y. S.; Zhang, Q. *Langmuir* **2011**, *27*, 1200−1206.
(9) Zhang, K.; Liang, J.; Wang, S.; Liu, J.; Ren, K. X.; Zheng, X.; Luo, H.; Peng, Y. J.; Zou, X.; Bo, X.; Li, J. H.; Yu, X. B. *Cryst. Growth Des.* **2012**, *12*, 793−803.
(10) Wang, Z. L.; Song, J. H. *Science* **2006**, *312*, 242−246.
(11) Xu, H. L.; Wang, W. Z. *Angew. Chem., Int. Ed.* **2007**, *46*, 1489−1492.
(12) Zhou, L.; Wang, W. Z.; Xu, H. L.; Sun, S. M.; Shang, M. *Chem.—Eur. J.* **2009**, *15*, 1776−1782.
(13) Cui, Y.; Lieber, C. M. *Science* **2001**, *291*, 851−853.
(14) Sun, S. H.; Murray, C. B.; Weller, D.; Folks, L.; Moser, A. *Science* **2000**, *287*, 1989−1992.
(15) Puntes, V. F.; Krishnan, K. M.; Alivisatos, A. P. *Science* **2001**, *291*, 2115−2117.
(16) Wang, X.; Zhuang, J.; Peng, Q.; Li, Y. D. *Nature* **2005**, *437*, 121−124.
(17) Tian, N.; Zhou, Z. Y.; Sun, S. G.; Ding, Y.; Wang, Z. L. *Science* **2007**, *316*, 732−735.
(18) Han, J. T.; Huang, Y. H.; Wu, X. J.; Wu, C. L.; Wei, W.; Peng, B.; Huang, W.; Goodenough, J. B. *Adv. Mater.* **2006**, *18*, 2145−2148.
(19) Song, J. M.; Mao, C. J.; Niu, H. L.; Shen, Y. H.; Zhang, S. Y. *CrystEngComm* **2010**, *12*, 3875−3881.
(20) Huo, Y. N.; Zhang, J.; Miao, M.; Jin, Y. *Appl. Catal., B* **2012**, *111−112*, 334−341.
(21) Zhang, X.; Ai, Z. H.; Jia, F. L.; Zhang, L. Z. *J. Phys. Chem. C* **2008**, *112*, 747−753.
(22) Feng, Y. C.; Li, L.; Li, J. W.; Wang, J. F.; Liu, L. *J. Hazard. Mater.* **2011**, *192*, 538−544.
(23) Henle, J.; Simon, P.; Frenzel, A.; Scholz, S.; Kaskel, S. *Chem. Mater.* **2007**, *19*, 366−373.
(24) Gnayem, H.; Sasson, Y. *ACS Catal.* **2013**, *3*, 186−191.
(25) Jiang, J.; Zhao, K.; Xiao, X. Y.; Zhang, L. Z. *J. Am. Chem. Soc.* **2012**, *134*, 4473−4476.
(26) Ye, L. Q.; Zan, L.; Tian, L. H.; Peng, T. Y.; Zhang, J. J. *Chem. Commun.* **2011**, *47*, 6951−6953.

(27) Han, X. G.; Jin, M. S.; Xie, S. F.; Kuang, Q.; Jiang, Z. Y.; Jiang, Y. Q.; Xie, Z. X.; Zheng, L. S. *Angew. Chem., Int. Ed.* **2009**, *48*, 9180−9185.
(28) Yang, H. G.; Sun, C. H.; Qiao, S. Z.; Zou, J.; Liu, G.; Smith, S. C.; Cheng, H. M.; Lu, G. Q. *Nature* **2008**, *453*, 638−641.
(29) Jiang, Z. Y.; Kuang, Q.; Xie, Z. X.; Zheng, L. S. *Adv. Funct. Mater.* **2010**, *20*, 3634−3645.
(30) Chen, L.; Yin, S. F.; Huang, R.; Zhou, Y.; Luo, S. L.; Au, C. T. *Catal. Commun.* **2012**, *23*, 54−57.
(31) Li, Y. Y.; Wang, J. S.; Yao, H. C.; Dang, L. Y.; Li, Z. J. *J. Mol. Catal. A* **2011**, *334*, 116−122.
(32) Yin, J. F.; Cao, H. Q.; Lu, Y. X. *J. Mater. Chem.* **2012**, *22*, 527−534.
(33) Yin, J. F.; Cao, H. Q.; Zhang, J. X.; Qu, M. Z.; Zhou, Z. F. *Cryst. Growth. Des.* **2013**, *13*, 759−769.
(34) Chen, L.; Yin, S. F.; Luo, S. L.; Huang, R.; Zhang, Q.; Hong, T.; Au, C. T. *Ind. Eng. Chem. Res.* **2012**, *51*, 6760−6768.
(35) Li, T. B.; Chen, G.; Zhou, C.; Shen, Y. Z.; Jin, R. C.; Sun, J. X. *Dalton Trans.* **2011**, *40*, 6751−6758.
(36) Wang, C. Y.; Zhang, H.; Li, F.; Zhu, L. Y. *Environ. Sci. Technol.* **2010**, *44*, 6843−6848.
(37) Wang, Y. N.; Deng, K. J.; Zhang, L. Z. *J. Phys. Chem. C* **2011**, *115*, 14300−14308.
(38) Cheng, H. F.; Huang, B. B.; Dai, Y.; Qin, X. Y.; Zhang, X. Y. *Langmuir* **2010**, *26*, 6618−6624.
(39) Hahn, N. T.; Hoang, S.; Self, J. L.; Mullins, C. B. *ACS Nano* **2012**, *6*, 7712−7722.